Chapter 3

Spacing Distributions

3.1 Introduction

Complex quantum systems from a wide variety of fields like quantum chaos, finance [43], econophysics [44], quantum chromodynamics [36], functional brain structures [88] and many more give rise to spectral fluctuations. It is very crucial to study these spectral fluctuations in order to understand the inherent complexities of complex quantum systems. These spectral fluctuations firstly reveal whether the given complex quantum system is in regular (or integrable) domain or in chaotic domain and they also describe the transition from regular to chaotic domain. In the context of quantum systems, the system is said to be integrable when we have knowledge of all the quantum numbers of the system, otherwise the system is said to be non-integrable or chaotic. In addition to this, they are also useful in characterizing distinct phases observed in physical systems such as localized or delocalized phase [89], insulating or metallic phase of many-body systems [90,91], integrable or chaotic limit of the underlying classical system [92] and low-lying shell model or mixing regime of nuclear spectra [55,93]. RMT is now established as a good model to describe these spectral fluctuations.

Over the years various measures have been developed in the field of RMT to study spectral fluctuations. Some of these measures give us knowledge about short-range correlations and others about long-range correlations between the energy-levels of the spectra of these systems. Among all these measures of RMT, one of the most popular and widely used is the nearest neighbor spacing distribution (NNSD) $P(s)$, which gives the degree of level repulsion. It tells us about the short-range correlations between nearest neighbors of energy-levels (or eigenvalues) of the complex quantum system. In 1984, Bohigas et al [37] conjectured that for a quantum system preserving time reversal and rotational symmetry

(represented by GOE), if a quantum system is chaotic then NNSD follows the Wigner surmise, which is the GOE result and it is given by,

$$P(s) = \frac{\pi}{2} s \exp\left(\frac{-\pi s^2}{4}\right) \tag{3.1}$$

This indicates the presence of 'level repulsion' and the energy levels are correlated. This was proved for certain systems by Haake et al [94]. On the other hand Berry and Tabor [95] established that if a quantum system is integrable, NNSD follows Poisson distribution, given by

$$P(s) = \exp(-s). \tag{3.2}$$

This displays 'level clustering' and the energy levels are uncorrelated. In order to construct NNSD for a given set of eigenvalues, we need to remove the variation in the density of eigenvalues. This is done using the procedure called unfolding [46, 55]. Recently the transition from regular to chaotic domain in wormholes and open quantum systems has been studied using NNSD [75, 96]. Going beyond the NNSD, higher-orders of these level spacings are also studied and the analytical expression for its distribution is derived in [97] using a Wigner-like surmise for Gaussian random matrix ensembles and also for Poisson ensemble.

Moving ahead, over the years various other measures in the field of RMT like number variance and spectral rigidity have been developed to study the long range correlations in these complex quantum systems [55, 98–100]. Complex systems can be represented in the form of a network and the spectral properties of these networks are now known to follow RMT. This opened a route to predict and control functional behavior of these complex systems [101, 102]. Now the short range correlations given by NNSD may give information only about the random connections in complex systems such as cancer networks. However, one can obtain further details about the underlying structural patterns in these systems if one studies long range correlations using measures like spectral rigidity [103]. Hence the long range correlation measures are also important along with short range correlation measures in the study of complex quantum systems. The intermediate distribution between Poisson and GOE was studied by Brody and hence called Brody distribution [104]. Recently, intermediate semi-poissonian statistics [105] and crossover random matrix ensembles [106] are also reported.

Going beyond this, recently Srivastava et. al. introduced another measures of spectral fluctuations called the distribution of the closest neighbor (CN) spacings, s_{CN} and farther neighbor (FN) spacings, s_{FN} from a given level [107]. The distribution of s_{CN} spacings is important in the context of perturbation theory, as the contribution from the closest neighbor

(CN) is prominent due to smaller energy spacing [108]. The distribution of s_{FN} spacings is complementary to that of s_{CN}. In [107], the analytical formulas for the distribution of CN and FN spacings are derived for GOE, GUE and GSE based on 3×3 matrix modeling and also for Poisson spectra. These analytical formulas are tested and found to be in very good agreement with the numerical results for the integrable circle billiard, fully chaotic cardioid billiard, standard map with chaotic dynamics and broken time reversal symmetry, and the zeros of the Riemann zeta function. In the first part of this chapter, we analyze the probability distributions of s_{CN} and s_{FN} using all the EGOE(1+2) ensembles for fermion and boson systems (with and without spin degree of freedom) which we have defined in chapter 2.

All the measures of spectral fluctuations discussed so far require the procedure of unfolding of the spectra in order to remove the secular variation in the density of eigenvalues [46, 55]. The unfolding is a cumbersome and non unique numerical procedure. Also, for many-body systems such as Bose-Hubbard model, unfolding procedure of the spectra becomes non-trivial as the density of states is not a smooth function of energy in the strong interaction domain [109–111]. Similarly, though in the nuclear shell model to a good approximation the density of states is close to an Edgeworth corrected Gaussian, in the interacting boson models of atomic nuclei, the smooth form of the density of states is not determined. Moreover, there are discrepancies between spectral and ensemble unfolding for non-ergodic random matrices [53, 55, 112]. In 2007 Oganesyan and Huse introduced a very good alternative to NNSD called the distribution of the ratio of consecutive level spacings $P(r)$ of the energy levels [109] and since then this method is gaining a lot of attraction [103, 113–117]. This is mainly because this method is simple to compute and no unfolding is needed as it is independent of the form of the density of the energy levels. The analytical expressions for $P(r)$ for the classical random matrix ensembles GOE, GUE and GSE were derived by Atas et. al [118]. Further these spacing ratios have been studied in finite many particle quantum systems modeled by embedded random matrix ensembles by Chavda and Kota [113]. This study established that for strong enough interactions they follow GOE results. The statistics of ratio of spacings has been used to quantify the distance from integrability on finite size lattices [110, 111], to investigate many-body localization [109, 119–121], to study spectral correlations in diffused van der Waals clusters [122] and to analyze spectra of uncorrelated random graph network [123]. More recently, exact distribution of spacing ratios for random and localized states in quantum chaotic systems is obtained using a 3×3 random matrix model with a possible correction term to it in [124].

Recently the higher orders of these spacing ratios have been studied in [125] and a generalized form of Wigner surmise has been proposed for the distribution of non-overlapping spacing ratios of higher-orders. This is shown for Gaussian and circular ensembles of RMT and for several physical systems such as spin chains chaotic billiards, Floquet systems and

measured nuclear resonances. It is important to note that in the past, a generalization of the Wigner surmise relation has been proposed between the higher order spacing distributions and NNSD [126, 127]. Also in [128], the higher order spacing distributions have been studied for systems with mixed regular chaotic dynamics. It is important to note that the ratio of two consecutive level spacings introduced by Oganesyan and Huse [109] in 2007 can be given in terms of s_{CN} and s_{FN} by $\tilde{r} = \frac{s_{CN}}{s_{FN}}$. In the second part of this chapter, we have analyzed the generic properties of non-overlapping higher order spacing ratios for various fermionic and bosonic embedded ensembles, with and without spin degree of freedom.

The Hamiltonian matrix H of a complex quantum system in finite dimensional space contains all information about the system. The nature of the matrix depends on various symmetries imposed on the system. In the presence of symmetries, the Hilbert space of the system splits into invariant subspaces giving block diagonal form for H. Each block is characterized by good quantum numbers corresponding to the respective symmetries. The spectral fluctuations of complex quantum systems are known to be consistent with that from random matrices, only for the discrete levels drawn from the same subspace. For mixed spectra, the levels from different blocks are superposed ignoring the symmetries, resulting in level clustering as the actual correlation between the levels is lost. This may give rise to misleading results since the level clustering is also a spectral signature of integrable systems [95]. Recently on the basis of rigorous numerical evidence, it is shown that using the higher order spacing statistics, in addition to the fluctuation characteristics, one can also obtain information about symmetry structure, for arbitrary sequence of measured or computed levels without desymmetrization [129]. Here desymmetrization means symmetry decomposition of the spectra of quantum systems. Recently this has also been studied in [130] using circular orthogonal, unitary and simplectic ensembles of RMT and the results are tested with three different physical systems viz. measured nuclear resonances, quantum chaotic kicked top and spin chains. With this result, it is also possible to analyze any arbitrary sequence of experimentally observed levels, whose symmetry structure is unknown. This method involves only the calculation of higher order spacing ratios and is straightforward compared to the complicated and approximate methods based on two-level cluster function for a composite spectrum [131, 132]. In the second part of this chapter, following the analysis of distribution of higher order spacing ratios, we also show that the quantitative information about the symmetry structure of the system can be obtained using higher order spacing ratios for embedded ensembles with spin degree of freedom.

Following this introductory section, the rest of the chapter is organized as follows. All the five different examples of EGOE(1+2) for fermion and boson systems with and without spin degree of freedom, used to analyze both the spacing distributions are given in section 3.2. The ordered level spacing distributions are introduced in section 3.3 along with their analytical results. The numerical results of ordered level spacing distributions are presented

in section 3.3.1. Further the higher order spacing ratios are defined in section 3.4. The numerical results of higher order spacing ratios are given in section 3.4.1. The quantitative information of the underlying symmetry structure in these systems is obtained using the distribution of higher order spacing ratios and these results are presented in section 3.4.2. The last section 3.5 gives conclusions of the entire analysis presented in this chapter. This chapter is based on [133] and [134].

3.2 EGOE Examples Used to Study Spacing Distributions

In this chapter in order to analyze two spacing distributions viz. ordered level spacing distribution and distribution of higher order spacing ratios, we consider the following five examples of EGOEs in many-particle spaces:

1. EGOE(1+2) with $m = 6$ and $N = 12$ resulting in matrix dimension of H is $d = 924$. The sp energies are chosen as $\epsilon_i = i + 1/i$, $i = 1, 2, ..., 12$ and the interaction strength is λ; For more details refer [24].

2. EGOE(1+2)-**s** with $m = 6$, $\Omega = 8$, $S = 0 - 3$ with matrix dimensions of H are 1176, 1512, 420 and 28 respectively. The sp energies are chosen as $\epsilon_i = i + 1/i$, $i = 1, 2, ..., 8$ and the interaction strength $\lambda = \lambda_0 = \lambda_1$; For more details refer [64, 135].

3. BEGOE(1+2) with $m = 10$ and $N = 5$ resulting in matrix dimension of H is $d = 1001$. The sp energies are chosen as $\epsilon_i = i + 1/i$, $i = 1, 2, ..., 5$ and the interaction strength is λ; For more details refer [27, 62].

4. BEGOE(1+2)-F with $m = 10$, $\Omega = 4$, and $F = 0 - 5$ with matrix dimensions of H are 196, 540, 750, 770, 594 and 286 respectively. The sp energies are chosen as $\epsilon_i = i + 1/i$, $i = 1, 2, 3, 4$ and the interaction strength $\lambda = \lambda_0 = \lambda_1$; For more details refer [22, 65].

5. BEGOE(1+2)-$S1$ with $m = 8$, $\Omega = 4$, $S = 0 - 8$ with matrix dimensions of H are 714, 1260, 2100, 1855, 1841, 1144, 840, 315 and 165 respectively. The sp energies are chosen as $\epsilon_i = i + 1/i$, $i = 1, 2, 3, 4$ and the interaction strength $\lambda = \lambda_0 = \lambda_1 = \lambda_2$; For more details refer [66].

Throughout this chapter, an ensemble of 500 members is used for all the examples to study both the spacing distributions. It is important to note that as λ increases in these EE,

(both fermion and boson), there is Poisson to GOE transition in level fluctuations at $\lambda = \lambda_C$ and Breit-Wigner to Gaussian transition in strength functions at $\lambda = \lambda_F > \lambda_C$. Also, they generate a third chaos marker at $\lambda = \lambda_t > \lambda_F$, a point or a region where thermalization occurs. In the region where $\lambda > \lambda_F$, there is enough mixing among the basis states and the system is in the Gaussian domain. For spinless fermion systems (i.e. EGOE(1+2)), $\lambda = 0.1$ is sufficiently large so that the system is in Gaussian domain [24]. Also, for fermions with spin degree of freedom, EGOE(1+2)-s is in Gaussian domain with $\lambda = 0.1$ [64, 135]. Similarly, for spinless bosons BEGOE(1+2) is in Gaussian domain for $\lambda = 0.06$ [27, 62]. For boson ensembles with spin degree of freedom, BEGOE(1+2)-F with $\lambda = 0.08$ [22,65] and BEGOE(1+2)-$S1$ with $\lambda = 0.2$ [66], again the systems exhibit GOE level fluctuations and the eigenvalue density as well as strength functions are close to Gaussian. The values of λ in all the ensemble calculations presented in this chapter are chosen sufficiently large so that there is enough mixing among the basis states and the system is in the Gaussian domain, i.e. $\lambda > \lambda_F$.

3.3 Ordered Level Spacing Distribution

In this section we define CN and FN spacings and give the analytical expressions of their probability distributions for both GOE and Poisson. Consider the set of unfolded eigenvalues e_n with $n = 1, 2, ..., d$ such that $e_1 < e_2 < ... < e_d$. Then the spacing between nearest neighbor levels can be given by $s_n = e_{n+1} - e_n$. Then, CN spacing is defined as $s_n^{CN} = \min\{s_{n+1}, s_n\}$ and the FN spacing is defined as $s_n^{FN} = \max\{s_{n+1}, s_n\}$. The probability distribution for the CN spacings and the FN spacings are represented by $P_{CN}(s)$ and $P_{FN}(s)$ respectively. If the system is in integrable domain then the form of NNSD gives Poisson distribution. Then $P_{CN}(s)$ and $P_{FN}(s)$ are given by,

$$P_{CN}^{P}(s) = 2\exp(-2s) \tag{3.3}$$

and

$$P_{FN}^{P}(s) = 2\exp(-s)[1 - \exp(-s)] \,, \tag{3.4}$$

respectively.

Similarly, if the system is in chaotic domain then the NNSD is GOE and is derived using 3×3 real symmetric matrices. Then $P_{CN}(s)$ and $P_{FN}(s)$ are given by [107],

$$
\begin{aligned}
P_{CN}^{GOE}(s) &= \tfrac{a}{\pi} s\ \exp(-2as^2)[3\sqrt{6\pi a}\ s - \pi \exp\left(\tfrac{3a}{2}s^2\right) \\
&\quad \times (as^2 - 3)\,\mathrm{erfc}(\sqrt{\tfrac{3a}{2}}\ s)]
\end{aligned}
\tag{3.5}
$$

and

$$
\begin{aligned}
P_{FN}^{GOE}(s) &= \tfrac{a}{\pi} s\ \exp(-2as^2)\ [\pi \exp\left(\tfrac{3a}{2}s^2\right) \\
&\quad \times (as^2 - 3)\ \{\mathrm{erf}(\sqrt{\tfrac{a}{6}}\ s) - \mathrm{erf}(\sqrt{\tfrac{3a}{2}}\ s)\} \\
&\quad + \sqrt{6\pi a}\ s(\exp\left(\tfrac{4a}{3}\ s^2\right) - 3)]
\end{aligned}
\tag{3.6}
$$

respectively.

Here $a = \frac{27}{8\pi}$. It is important to note that $2P(s) = P_{CN}(s) + P_{FN}(s)$. For small spacings s, $P_{CN}^{GOE}(s)$ shows level-repulsion similar to the NNSD and $P_{FN}^{GOE}(s) \propto s^4$. While for large s, $P_{FN}^{GOE}(s) \propto \exp\left(\frac{-2a}{3}s^2\right)$. For GOE, the average value $\langle s_{CN} \rangle = \frac{2}{3}$ and for Poisson it is $\frac{1}{2}$. However, the average value $\langle s_{FN} \rangle = \frac{4}{3}$ for GOE and $\frac{3}{2}$ for Poisson.

In this chapter, we have studied spectral fluctuations in EE for fermion and boson systems with and without spin degree of freedom using P_{CN} and P_{FN}. We present the numerical results in the next section.

3.3.1 Numerical Results

In this section the probability distributions of CN and FN spacings for all the EGOE(1+2) examples given in section 3.2 are constructed using the following procedure. To construct these distributions we first need to carry out the procedure of unfolding of the spectrum, in order to remove the variation in the density of eigenvalues. In this chapter, the unfolding of the spectrum is done using the procedure used in [112], with the smooth density as a corrected Gaussian with corrections involving up to 4-6th order moments of the density function so that the average spacing is unity. The process of unfolding is done separately for each member. Then the numerical histograms are constructed for $P_{CN}(s)$ and $P_{FN}(s)$ using the central 80% part of the spectrum with the bin size equal to 0.1. We have also computed the ensemble averaged skewness (γ_1) and excess (γ_2) parameters which are shown in Table 3.1 for all the examples of EE analyzed in this chapter. Now first let us consider EE without spin degree of freedom. The histograms in Fig. 3.1 present the $P_{CN}(s)$ and $P_{FN}(s)$ results for EE without spin degree of freedom, EGOE(1+2) (for fermions) and BEGOE(1+2) (for bosons). Moving further with spin degree of freedom, Fig. 3.2 presents the EE results with spin degree of freedom, EGOE(1+2)- s (for fermions) and

BEGOE(1+2)-F and BEGOE(1+2)-$S1$ (for bosons). All these numerical ensemble averaged results are compared with the theoretical predictions (red continuous curves) given by Eqs.(3.5) and (3.6) for all the examples in these figures and a very good agreement is observed between them. Also, the ensemble averaged values of $\langle s_{CN} \rangle$ and $\langle s_{FN} \rangle$ are calculated for all these examples and are given in Table 3.2. They are found to be very close to corresponding GOE estimates. In addition to this, we have also analyzed shell model example which is a typical member of EGOE(1+2)-JT [24]. In literature this ensemble is usually known as TBRE [54]. The result is shown in Fig. 3.3. Here also the shell model results along with the calculated averages are consistent with the theoretical predictions.

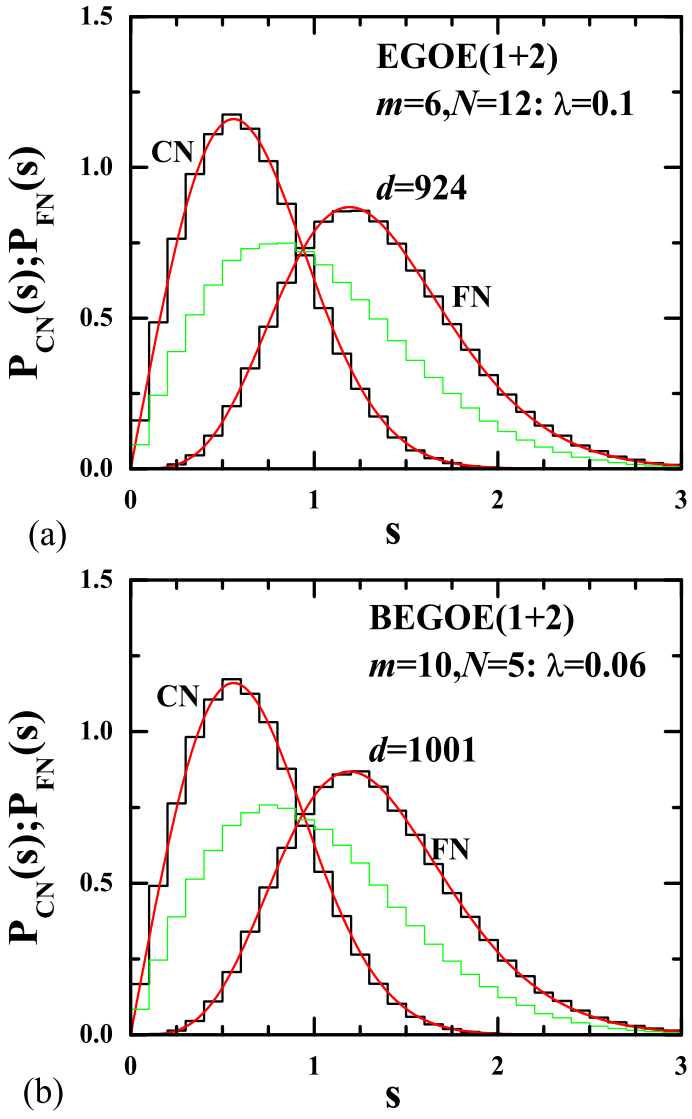

Figure 3.1: Black histograms represent the probability distribution of closest neighbor spacings $P_{CN}(s)$ and farther neighbor spacings $P_{FN}(s)$ for a 500 member (a) EGOE(1+2) ensemble and (b) BEGOE(1+2) ensemble. The red smooth curves are obtained using Eqs. (3.5) and (3.6). The NNSD is shown by green histogram for comparison.

Past studies have shown that EGOE(1+2) and BEGOE(1+2) ensembles exhibit a Poisson to GOE transition in level fluctuations with increase in the strength of the two-body

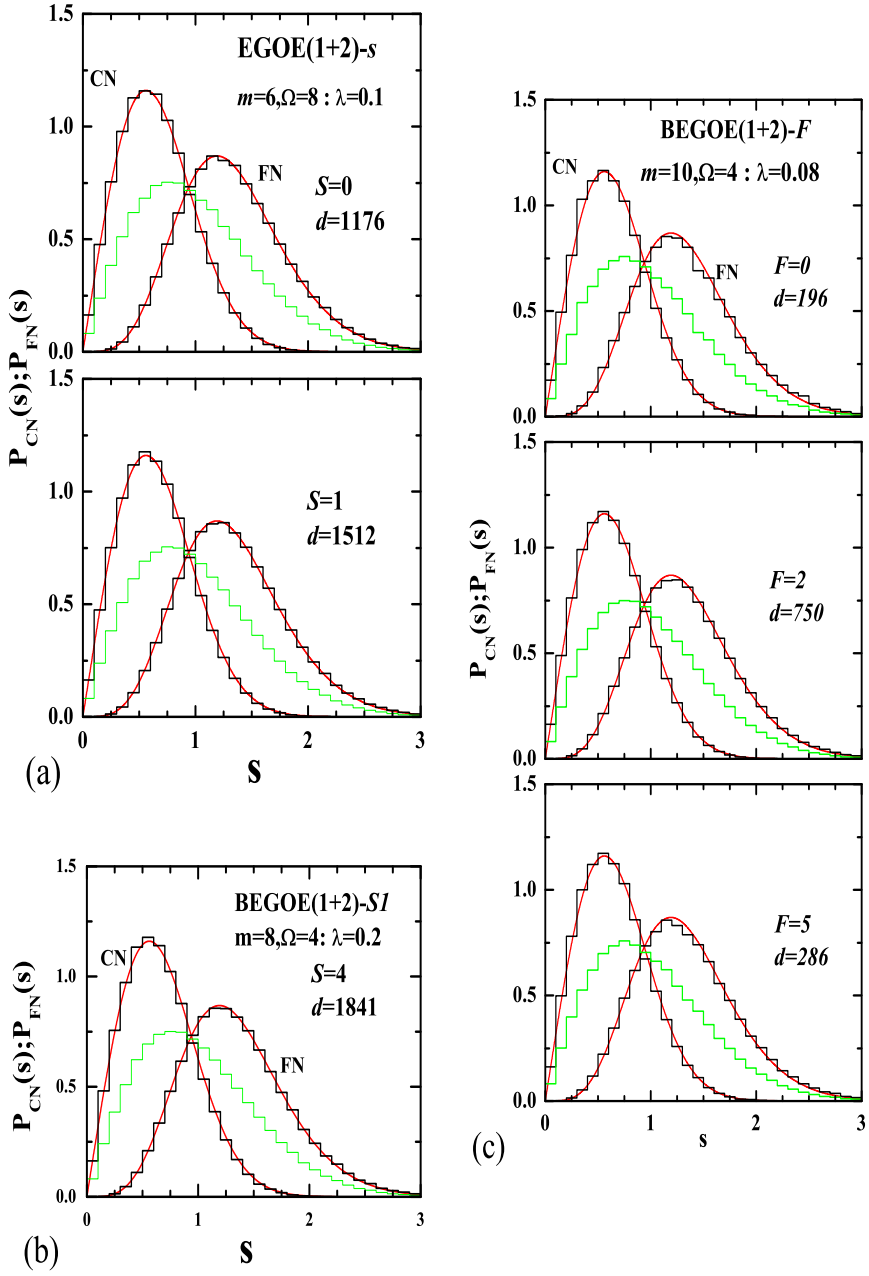

Figure 3.2: The probability distribution of closest neighbor spacings $P_{CN}(s)$ and farther neighbor spacings $P_{FN}(s)$ for (a) EGOE(1+2)- s ensemble for spin values $S = 0$ and 1 (b) BEGOE(1+2)- $S1$ ensemble for spin value $S = 4$ and (c) BEGOE(1+2)- F ensemble for spin values $F = 0, 2$ and 5. See Fig. 3.1 and text for details.

interaction λ [24, 62, 65, 115, 135]. It is also possible to study this Poisson to GOE transition in terms of $\langle s_{CN} \rangle$ and $\langle s_{FN} \rangle$. We have computed $\langle s_{CN} \rangle$ and $\langle s_{FN} \rangle$ for spin-less fermion and boson ensembles by varying the interaction strength λ and the results are shown in Fig. 3.4. It is clearly seen that for lower values of λ, the values of $\langle s_{CN} \rangle$ and $\langle s_{FN} \rangle$ are close to Poisson, which gradually reach the GOE value with increase in

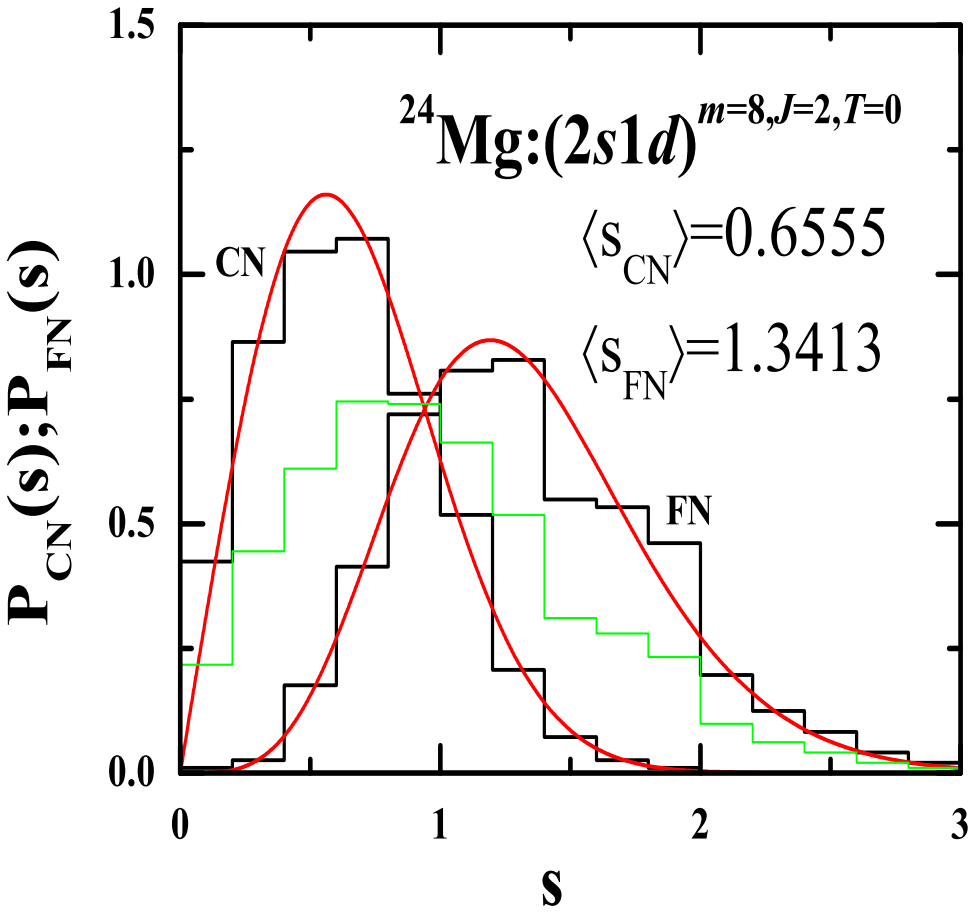

Figure 3.3: The probability distribution of closest neighbor spacings $P_{CN}(s)$ and farther neighbor spacings $P_{FN}(s)$ vs. s for Nuclear shell model example: ^{24}Mg with 8 nucleons in the $(2s1d)$ shell with angular momentum $J = 2$ and isospin $T = 0$. The matrix dimension is 1206 and all levels are used in the analysis. See Ref. [112] for further details. The skewness and excess parameters are $\gamma_1 = 0.139$ and $\gamma_2 = -0.061$. $\langle s_{CN}\rangle$ and $\langle s_{FN}\rangle$ values are also given in the figure.

λ. Therefore, there is a transition from Poisson to GOE form in $P_{CN}(s)$ (and also in $P_{FN}(s)$). With this it is possible to define a chaos marker λ_C such that for $\lambda > \lambda_C$, the level fluctuations follow GOE. This transition occurs when the interaction strength λ is of the order of the spacing Δ between the states that are directly coupled by the two-body interaction. In the past, the NNSD [136] and the distribution of ratio of consecutive level spacings [114] have been used to study Poisson-to-GOE transition by constructing suitable random matrix model and the transition parameters were used to identify the chaos marker λ_C in the EE [24, 62, 65, 115, 135]. Corresponding to the critical values of these transition parameters required for onset of GOE fluctuations, we found the critical value of $\langle s_{CN}\rangle$, $\langle s_{CN}\rangle_C = 0.62$ (and $\langle s_{FN}\rangle_C = 1.38$). This is represented by blue dotted lines in Fig. 3.4. $\langle s_{CN}\rangle_C = 0.62$ gives $\lambda_C \simeq 0.028$ for EGOE(1+2) example and $\lambda_C \simeq 0.024$ for BEGOE(1+2) example. These values are shown by dashed vertical lines in Fig. 3.4 and are close to the previously obtained results [31, 115]. These results show that, these measures

can also be used to identify λ_C marker using $P_{CN}(s)$ and $P_{FN}(s)$.

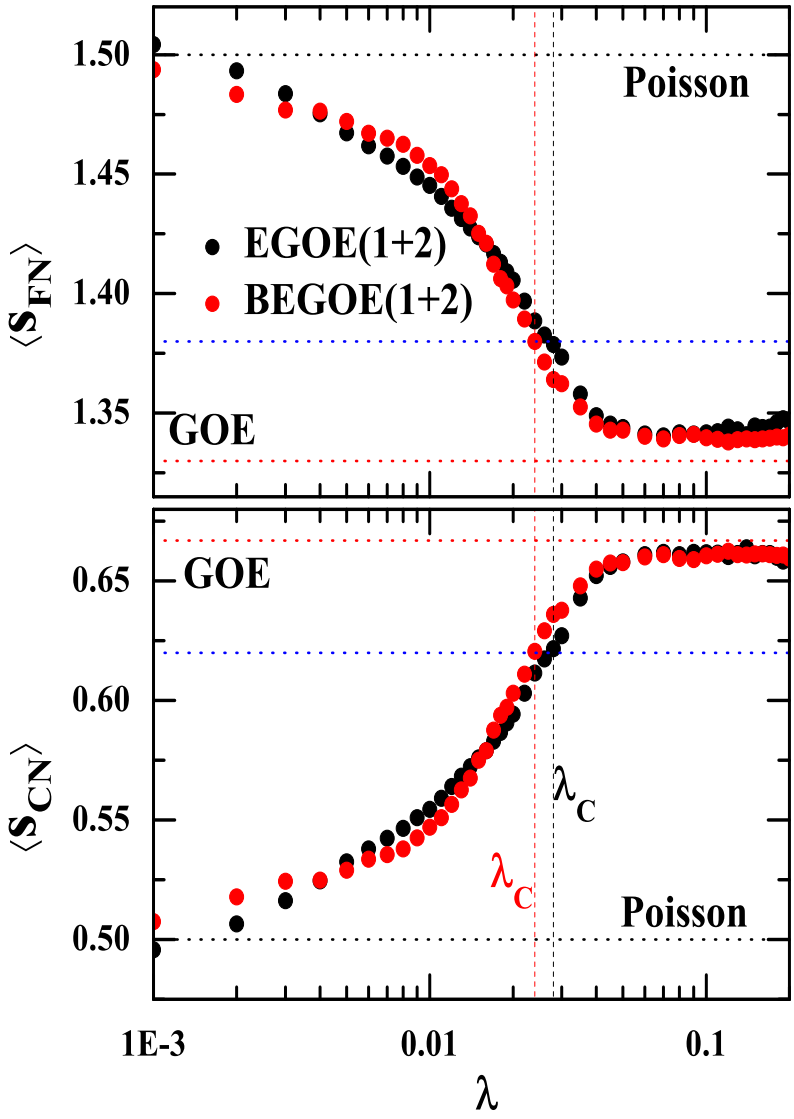

Figure 3.4: Ensemble averaged values of $\langle s_{CN}\rangle$ (lower panel) and $\langle s_{FN}\rangle$ (upper panel) as a function of the two-body strength of interaction λ, obtained for EGOE(1+2) ensemble with $(m, N) = (6, 12)$ (black circles) and BEGOE(1+2) ensemble with $(m, N) = (10, 5)$ (red circles). In the calculations sp energies are drawn from the center of a GOE. The vertical dash-lines represent the position of λ_C for the corresponding EGOE(1+2) and BEGOE(1+2) examples. In each calculation, an ensemble of 500 members is used. The horizontal dotted-lines represent Poisson estimate (black), GOE estimate (red) and $\langle s_{CN}\rangle_C = 0.62$ (and $\langle s_{FN}\rangle_C = 1.38$). See text for further details.

3.4 Distribution of Higher Order Spacing Ratios

Let us consider the set of eigenvalues E_n with $n = 1, 2, ..., d$ such that $E_1 < E_2 < ... < E_d$. The consecutive eigenvalue spacings are given by $s_n = E_{n+1} - E_n$. The ratios

Table 3.1: The ensemble averaged values of parameters γ_1 (skewness) and γ_2 (excess) for various embedded ensemble examples used in this chapter.

Embedded Ensemble	γ_1	γ_2
EGOE(1+2)	0.0008	-0.3431
EGOE(1+2)-s		
$S = 0$	0.0202	-0.3034
$S = 1$	0.0178	-0.3352
BEGOE(1+2)	0.0922	-0.2329
BEGOE(1+2)-F		
$F = 0$	0.0088	-0.3114
$F = 2$	0.0469	-0.3129
$F = 5$	0.0677	-0.2569
BEGOE(1+2)-$S1$		
$S = 4$	0.0349	-0.1111

Table 3.2: Average values of the closest neighbor spacings ($\langle s_{CN} \rangle$) and farther neighbor spacings ($\langle s_{FN} \rangle$) obtained numerically for various embedded ensemble examples used in this chapter. Theoretical average values for Poisson and GOE are also given.

Embedded Ensemble	$\langle s_{CN} \rangle$	$\langle s_{FN} \rangle$
EGOE(1+2)	0.6613	1.3417
EGOE(1+2)-s		
$S = 0$	0.6616	1.3411
$S = 1$	0.6625	1.3409
BEGOE(1+2)	0.6600	1.3401
BEGOE(1+2)-F		
$F = 0$	0.6585	1.3421
$F = 2$	0.6600	1.3404
$F = 5$	0.6578	1.3420
BEGOE(1+2)-$S1$		
$S = 4$	0.6600	1.3401
Poisson	$\frac{1}{2}$	$\frac{3}{2}$
GOE	$\frac{2}{3}$	$\frac{4}{3}$

of two nearest neighbor or consecutive eigenvalue spacings are given by $r_n = s_{n+1}/s_n$. For GOE, using an exact calculation for 3×3 real symmetric matrices, the probability distribution $P(r)$ for consecutive eigenvalue spacings is derived to be given by Wigner-

like surmise [118],

$$P_W(r) = \frac{27}{8}\frac{(r+r^2)}{(1+r+r^2)^{5/2}} \ . \tag{3.7}$$

On the other hand if the quantum system is in integrable domain the probability distribution $P(r)$ is given by,

$$P_P(r) = \frac{1}{(1+r)^2} \ . \tag{3.8}$$

Nearest neighbor spacing ratios r probe fluctuations in spectral scales of the order of unit mean spacing. Many different variants of consecutive level spacing ratios have been studied recently [113, 114, 124].

Now let us define the non-overlapping higher order spacing ratios such that there is no shared eigenvalue spacing in the numerator and denominator. They are given as,

$$r_n^{(k)} = \frac{s_{n+k}^{(k)}}{s_n^{(k)}} = \frac{e_{n+2k} - e_{n+k}}{e_{n+k} - e_n}; \ \ n, k = 1, 2, 3... \tag{3.9}$$

Higher order spacing ratios $r^{(k)}$ probe fluctuations in spectral interval of k mean spacings. Let $P^k(r)$ denote the non-overlapping k-th order probability distribution. Recently, for the random matrices, belonging to the Gaussian and circular ensembles of RMT, it is shown that there exists an elegant scaling relation between non-overlapping k-th order spacing ratio distribution and the nearest neighbor spacing ratio distribution [125]. For GOE random matrices applicable to Hamiltonians with time-reversal invariance, non-overlapping k-th order spacing ratio distribution $P^k(r)$ is identical to the nearest neighbor spacing ratio distribution $P_\alpha(r)$ with scaling parameter α and its functional form is given by [125],

$$\begin{aligned} P^k(r) = P_\alpha(r) &= C_\alpha \frac{(r+r^2)^\alpha}{(1+r+r^2)^{1+3\alpha/2}} \ , \\ \alpha &= \frac{(k+2)(k+1)}{2} - 2, k \geq 1 \ . \end{aligned} \tag{3.10}$$

Here C_α is a normalization constant. The scaling parameter $\alpha \geq 4$ can take large integer values and it accounts for the dependence on order k of the spacing ratio. On the other hand if the quantum system is in integrable domain, non-overlapping k-th order spacing ratio distribution $P^k(r)$ is given by,

$$P_P^k(r) = \frac{(2k-1)!}{[(k-1)!]^2}\frac{r^{k-1}}{(1+r)^{2k}}. \tag{3.11}$$

Note that we have $P(r) = P^1(r) = P_1(r)$. This means that $k = 1$ gives the $P(r)$ distribution. The generalized scaling relation holds good for Gaussian and circular ensembles

of RMT and for several physical systems such as spin chains, chaotic billiards, Floquet systems and measured nuclear resonances [125]. Also in [125], the finite size effect and different rate of convergence of the scaling relation are discussed as well using various examples. It is also useful if we compute the average values of spacing ratios r which is given by $\langle r\rangle = \int r\, P^k(r)\, dr$. In a similar manner, we can compute the average values of spacing ratios $\langle r\rangle_\alpha$ using $P_\alpha(r)$. The values of $\langle r\rangle_\alpha$ corresponding to $k = 2,\ 3$ and 4 are 1.1747, 1.0855 and 1.0521 respectively. $P^k(r)$, $P_\alpha(r)$ and $\langle r\rangle$ are used in the analysis of energy levels presented in Section 3.4.1. In this chapter we analyze $P^k(r)$ for EE for fermion and boson systems with and without spin degree of freedom and these numerical results are presented in the next section.

3.4.1 Numerical Results

Using the definition of higher order spacing distributions given in Section 3.4, we have constructed k-th order spacing ratio distribution $P^k(r)$ for all the EGOE(1+2) models defined in chapter 2. The numerical histograms for $P^k(r)$ are constructed for $k = 2,\ 3$ and 4 using the central 80% of the spectrum. A bin-size of 0.1 is chosen for this entire analysis. The $P^k(r)$ results for EE for fermion and boson systems without spin degree of freedom using EGOE(1+2) and BEGOE(1+2) respectively are presented in Fig. 3.5. The black histograms correspond to the ensemble averaged numerical results and they are compared with $P_\alpha(r)$ (smooth red curves) given by Eq. (3.10). For $k = 2, 3$ and 4 the corresponding α values are 4, 8 and 13 respectively. we have also computed the ensemble averaged values of spacing ratios, $\langle r\rangle$, and they are shown in the figure. Going beyond the spinless systems, Fig. 3.6 presents $P^k(r)$ results for $k = 2$, 3 and 4 for EE with spin degree of freedom using EGOE(1+2)-s for fermions and for bosons using BEGOE(1+2)-F and BEGOE(1+2)-$S1$. The ensemble averaged numerical results (black histograms) are compared with $P_\alpha(r)$ (smooth red curves) given by Eq. (3.10). For all the examples of EE, we find that $\langle r\rangle_{EE} \sim \langle r\rangle_\alpha$. The results presented in Figs. 3.5 and 3.6, show an excellent agreement between numerical histograms and $P_\alpha(r)$ establishing the universal feature of Eq. (3.10) in explaining the higher order spacing ratios in many-body interacting quantum systems, with and without spin degree of freedom. Now we know that when we include all the levels in the analysis, the NNSD gets affected by the choice of unfolding function. However when we analyze the distribution of higher order spacing ratios by including all the levels, we obtain a good agreement between $P^k(r)$ and $P_\alpha(r)$. In the past it is shown that the energy levels of EGOE(1+2) close to the ground state (tails of the energy spectrum) generate large fluctuations compared to that of GOE fluctuations. This is shown using NNSD [137] and also using $P(r)$ [113]. Going further, it is interesting to test the validity of Eq. (3.10) close to the ground state. The numerical histograms for these are

compared with $P_\alpha(r)$ (smooth red curves) in Fig. 3.7. The results show a clear deviation between embedded ensemble $P^k(r)$ and $P_\alpha(r)$ from the trend predicted by Eq. (3.10) and deviations increasing with increasing k. Also, $\langle r \rangle_{EE}$ values are found to be smaller than the corresponding $\langle r \rangle_\alpha$ values. Therefore, although one need not exclude the spectrum tails while analyzing non-overlapping spacing ratios, Eq. (3.10) does not explain the variation in spacing ratios close to the ground state.

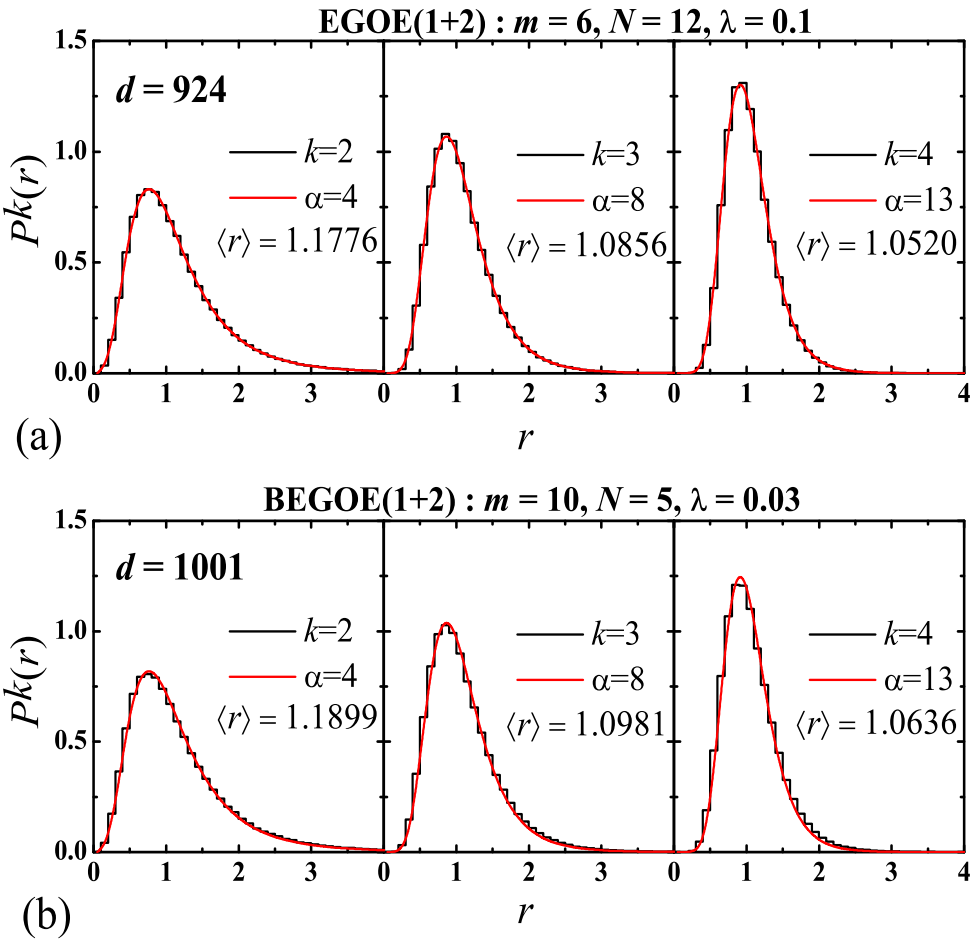

Figure 3.5: Probability distribution of the k-th order spacing ratios $P^k(r)$ vs. r for a 500 member (a) EGOE(1+2) ensemble and (b) BEGOE(1+2) ensemble with $k = 2$, 3, and 4. Black histograms correspond to the numerical results and the red smooth curves represent $P_\alpha(r)$ obtained using Eq. (3.10) with α values as mentioned in each panel.

3.4.2 Symmetry Structure

The distribution of non-overlapping higher-order spacing ratios discussed in the previous sections is not only useful in explaining universal features of fluctuation characteristics but also to reveal quantitative information regarding underlying symmetry structure of the given complex quantum system. As conjectured by Dyson [41] and proved by Gunson [138], the spectral statistics of two superposed circular orthogonal ensemble (COE)

spectra converge to that of circular unitary ensemble (CUE). This is expected to be echoed in the distribution of level spacings and spacing ratios as well. In [129] it has been demonstrated that distribution of higher order spacing ratios carry symmetry information with the help of various examples like superposed GOE spectra, billiards, spin-$1/2$ chains and neutron resonance data.

We begin with an arbitrary sequence of eigenvalues of GOE Hamiltonian H, which is a superposition of $\mathbf{m}$ blocks. Here each block is characterized by good quantum numbers. Then, in this case we denote the distribution of non-overlapping k-th order spacing ratios by $P^k(r,\mathbf{m})$. Here $P^k(r,\mathbf{m})$ converges to $P_\alpha(r)$ [129], in the same way as Eq.(3.10),

$$P^k(r,\mathbf{m}) = P_\alpha(r) \text{ when } \alpha = k = \mathbf{m}. \tag{3.12}$$

Note that, here $P^k(r,\mathbf{m}=1) = P^k(r)$. Therefore, the validity of Eq.(3.12) implies that in addition to their fluctuation properties $P^k(r)$ can also reveal the information about the symmetry structure of the composite spectra of complex quantum systems. In this chapter we show this using EE with spin degree of freedom using Eq.(3.12). This has direct applications in the analysis of nuclear energy levels giving information about isospin and F-spin. We have seen in chapter 2 that EE models with spin for fermion and boson systems i.e. EGOE(1+2)-$\mathbf{s}$, BEGOE(1+2)-F and BEGOE(1+2)-$S1$, have specific spin structure: for EGOE(1+2)-$\mathbf{s}$ and BEGOE(1+2)-F, the random interaction matrix $V(2)$ in two-particle spaces is a direct sum of matrices in spin 0 and 1 channels; and for BEGOE(1+2)-$S1$, the $V(2)$ matrix in two-particle spaces is a direct sum of matrices in spin 0, 1 and 2 channels. The many-particle Hamiltonian matrix is a block diagonal matrix with each block corresponding to EGOE(1+2) with a given spin S. It is interesting to investigate if signatures of these spin structures are reflected in $P^k(r)$. In order to study this, we superpose $\mathbf{m}$ independent spin blocks and compare non-overlapping k-th order spacing ratio distribution $P^k(r,\mathbf{m})$ with $P_\alpha(r)$ given by Eq. (3.10). The results presented in Figs. 3.8-3.10 correspond to EGOE(1+2)-$\mathbf{s}$, BEGOE(1+2)-F and BEGOE(1+2)-$S1$ examples discussed in section 3.2. In these figures, the ensemble averaged histograms for $P^k(r,\mathbf{m})$ are obtained by arranging the spectra of $\mathbf{m}$ spin blocks in ascending order for each member of the ensemble. Then, ensemble average is computed and plotted as a histogram with bin-size of 0.1 for all k values. The results in the upper panel of Fig. 3.8 are for $P^k(r,\mathbf{m})$ with $\mathbf{m}=2$ obtained by superposing spectra corresponding to $S=0$ and $S=1$ while that in the lower panel are with $\mathbf{m}=3$ obtained by superposing spectra corresponding to $S=0$, $S=1$ and $S=2$. The smooth red curves are for $P_\alpha(r)$ obtained using Eq. (3.10) with α values shown in each panel. A very good agreement between ensemble averaged $P^k(r,\mathbf{m})$ results and $P_\alpha(r)$ is found for $\alpha = k = \mathbf{m}$ implying that the condition given by Eq. (3.12) is satisfied. There are clear deviations for all other values. This confirms the presence of $\mathbf{m}$ symmetries. Similarly, results in Figs. 3.9 and 3.10 also show excellent agreement between

ensemble averaged k-th order spacing ratio distribution and nearest neighbor spacing ratio results given by Eq. (3.10) with $\alpha = k = \mathbf{m}$ confirming the presence of $\mathbf{m}$ symmetries.

In order to obtain the best quantitative estimate for α, we calculate χ^2 measure defined as,

$$\chi^2(\alpha) = \log\left\{\int_0^\infty dr(P^k(r,\mathbf{m}) - P_\alpha(r))^2\right\} \ . \tag{3.13}$$

Here, minimum value of $\chi^2(\alpha)$ implies $P^k(r,\mathbf{m}) \sim P_\alpha(r)$. Fig. 3.11 shows the variation in $\chi^2(\alpha)$ as a function of α for various $\mathbf{m}$ values. The left panel gives the results for EGOE(1+2)-$\mathbf{s}$ and the right panel gives the results for BEGOE(1+2)-F. We have not included spectra of maximum spin $S = S_{max}$ for EGOE (1+2)-$\mathbf{s}$ and spectra of minimum spin $F = F_{min}$ for BEGOE(1+2)-F due to small matrix dimensions. The minimum value for $\chi^2(\alpha)$ is obtained at $\alpha = k = \mathbf{m}$, which is in agreement with the results shown in Figs. 3.8 and 3.9. We have also confirmed this result with other combinations of superposed spectra corresponding to different spin sectors. It is important to note that similar results were obtained by combining $\mathbf{m}$ blocks of EGOE and GOE spectra. Therefore, the distribution of higher order level spacing ratios are independent of the state density of the spectra and can also be useful in extracting symmetry information of the composite spectra. There are deviations from obtaining minimum for $\chi^2(\alpha)$ at $\alpha = k = \mathbf{m}$ when the dimension of a given spin block is very small. Fig. 3.12 shows variation in $\chi^2(\alpha)$ as a function of α for EGOE(1+2)-$\mathbf{s}$ (top left panel), BEGOE(1+2)-F (middle left panel) and BEGOE(1+2)-$S1$ (bottom left panel). Results are shown for various $\mathbf{m}$ values. For EGOE (1+2)-$\mathbf{s}$, the minimum for $\chi^2(\alpha)$ is not at $\alpha = k = \mathbf{m}$ for $\mathbf{m} = 4$ as it is obtained by superposing four spin blocks corresponding to $S = 0-3$. Here, $S = 3$ is the maximum allowed spin and has the smallest dimension (28 compared to dimensions 1176, 1512, 420 respectively for spins $S = 0$, $S = 1$ and $S = 2$). Similarly, deviations are seen in minimum for $\chi^2(\alpha)$ from $\alpha = k = \mathbf{m}$ at $\mathbf{m} = 6$ for BEGOE(1+2)-F and for $\mathbf{m} = 6-9$ for BEGOE(1+2)-$S1$. Going further, we superposed $\mathbf{m}$ GOE spectra of exact same dimensions (see Fig.3.12) corresponding to EGOE(1+2)-$\mathbf{s}$ (top right panel), BEGOE(1+2)-F (middle right panel) and BEGOE(1+2)-$S1$ (bottom right panel). These results also show similar deviations in minimum for $\chi^2(\alpha)$ confirming that there are finite-size effects.

Similar set of calculations have been performed for BEGOE(1+2) and BEGOE(1+2)-F with $\lambda = 0.06$ and $\lambda = 0.08$ respectively, such that the system is in Gaussian domain [22, 27, 62, 65]. These calculations also give similar results.

3.5 Conclusions

In this chapter we have studied spectral fluctuations in interacting fermion and boson systems with and without spin degree of freedom using two spacing distributions. In first part of this chapter, we have studied the probability distribution of closest neighbor spacings $P_{CN}(s)$ and the farther neighbor spacings $P_{FN}(s)$. In the past studies it has been shown that EE exhibit GOE level fluctuations only with proper spectral unfolding. Our numerical results for various examples of fermion and boson system and shell model, are consistent with the recently derived analytical expressions using a 3×3 random matrix model and other related quantities [107]. This establishes the universality of these analytical expressions. Also, it shows that for strong enough interaction, the local level fluctuations generated by EE follow the results of classical Gaussian ensembles.

The ordered level spacing distribution involves the cumbersome and non-unique procedure of unfolding to remove the variation in the density of states. A good escape from this process of unfolding is to use the method of distribution of ratio of consecutive level spacings $P(r)$ introduced by Oganesyan and Huse. This method does not require the unfolding process as it is independent of the form of the density of the energy levels. In the second part of this chapter, the probability distribution of non-overlapping spacing ratios of higher orders $P^k(r)$ are studied. We have obtained excellent agreement between numerical results for higher order spacing ratios and recently derived Wigner surmise like scaling relation. Thus, this scaling relation is universal to understand higher order spacing ratios in such systems. Moving further, we have also shown that these higher order spacing ratio distributions can also reveal quantitative information about underlying symmetry structure in these systems. This shows that the analysis of higher order spacing ratios is not only useful in studying spectral fluctuations but also reveals quantitative information about symmetry structure of complex quantum systems.

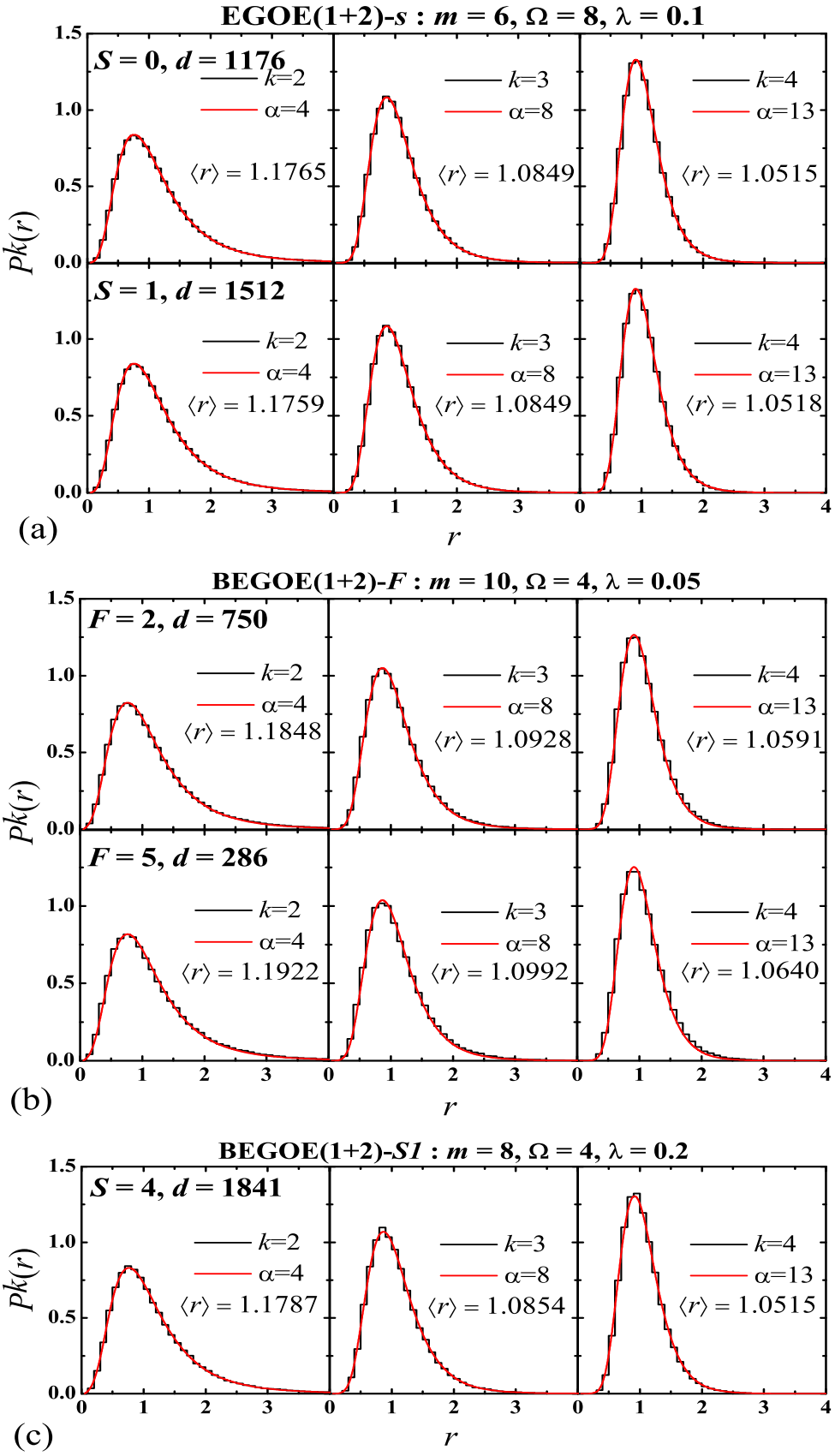

Figure 3.6: Same as Fig. 3.5 but results are for a 500 member (a) EGOE(1+2)- s (b) BEGOE(1+2)- F and (c) BEGOE(1+2)- $S1$. See text for details.

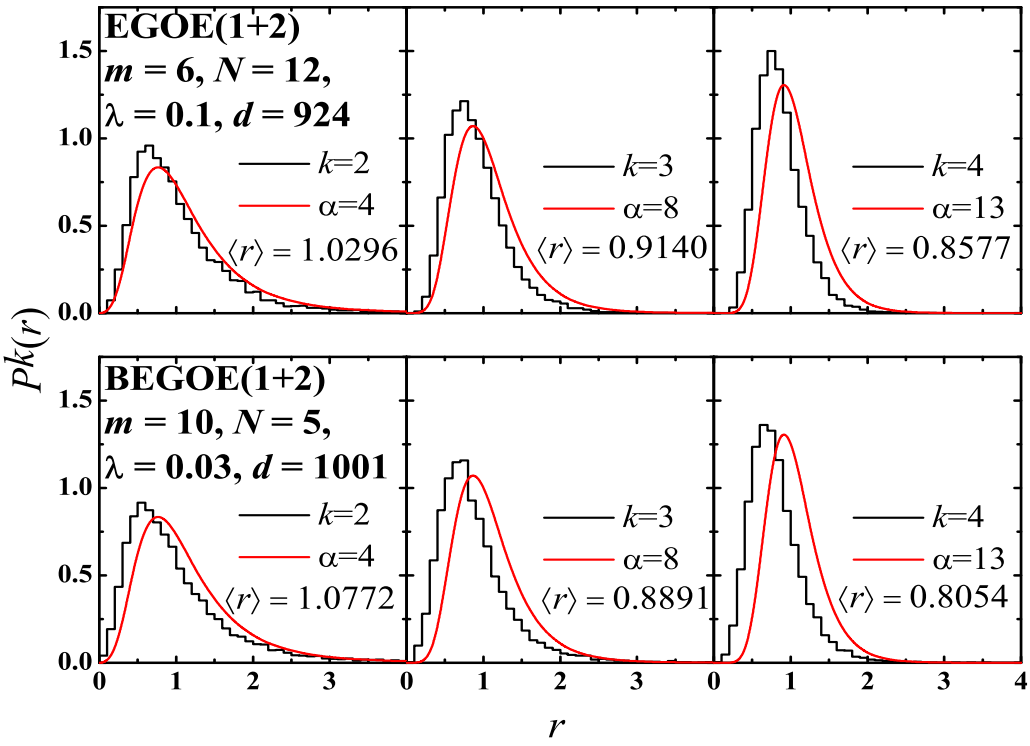

Figure 3.7: Histograms represent probability distribution $P^k(r)$ of the k-th order spacing ratios for the lowest 20 energy levels using EGOE(1+2) (top panel) and BEGOE(1+2) (bottom panel) ensembles. The red smooth curves are obtained using Eq. (3.10) with α values as mentioned in each panel.

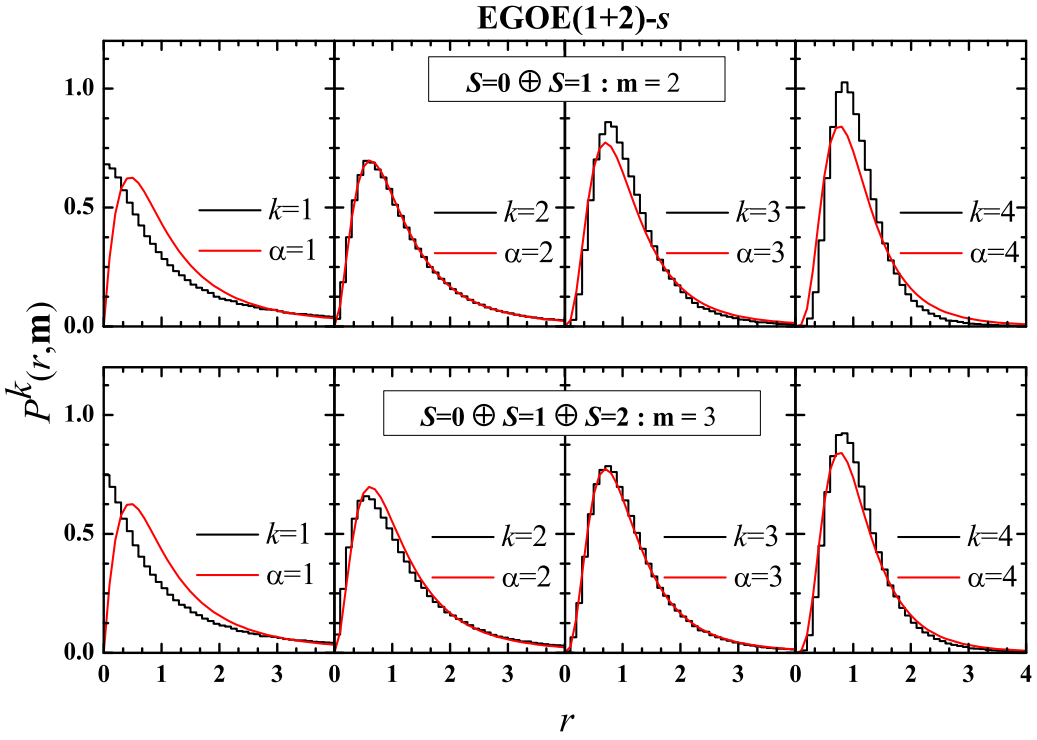

Figure 3.8: Probability distribution of non-overlapping k-th order spacing ratios of $\mathbf{m}$ independent superposed spin blocks $P^k(r, \mathbf{m})$ for a 500 member EGOE(1+2)- $\mathbf{s}$ ensemble. Here $\lambda = \lambda_0 = \lambda_1 = 0.1$. Results for $\mathbf{m} = 2$, with spins $S = 0 - 1$ are shown in the upper panel and results for $\mathbf{m} = 3$, with spins $S = 0 - 2$ are shown in lower panel. The histograms corresponding to the numerical results are compared with the red smooth curves obtained using Eq. (3.10) with α values as mentioned in each panel.

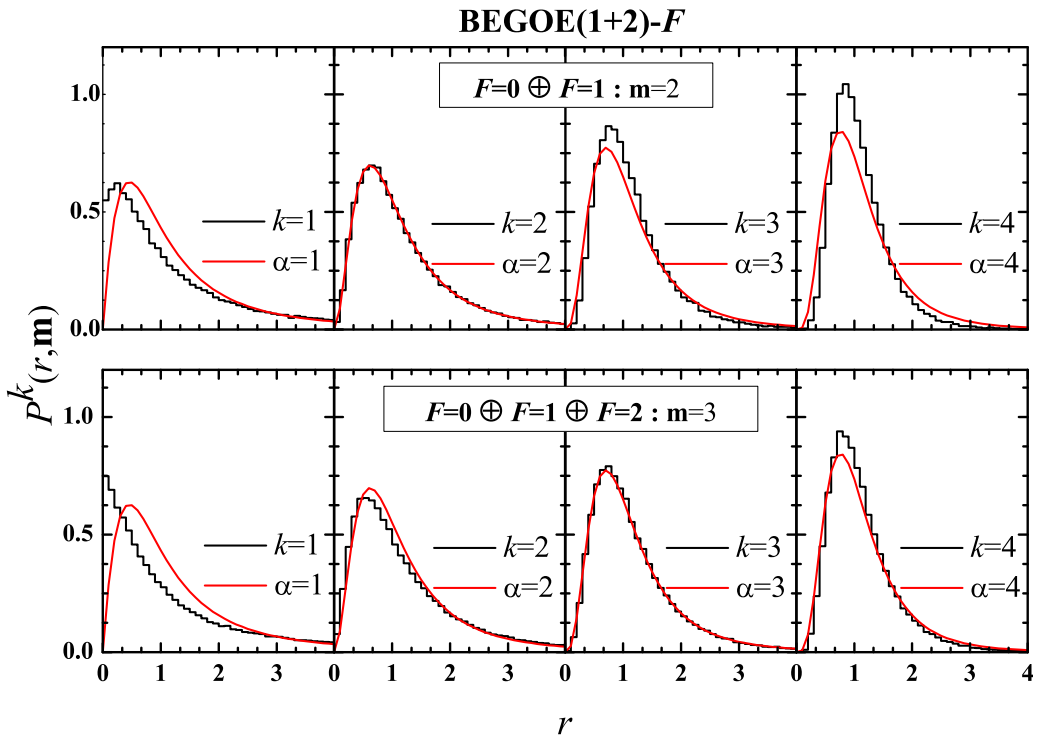

Figure 3.9: Same as Fig. 3.8 but results are for $\mathbf{m}$ superposed spectra of a 500 member BEGOE(1+2)-F ensemble. Here $\lambda = \lambda_0 = \lambda_1 = 0.05$. Results for $\mathbf{m} = 2$ with spins $F = 0 - 1$ are shown in upper panel and results for $\mathbf{m} = 3$ with spins $F = 0 - 2$ are shown in lower panel. See Fig. 3.8 for details.

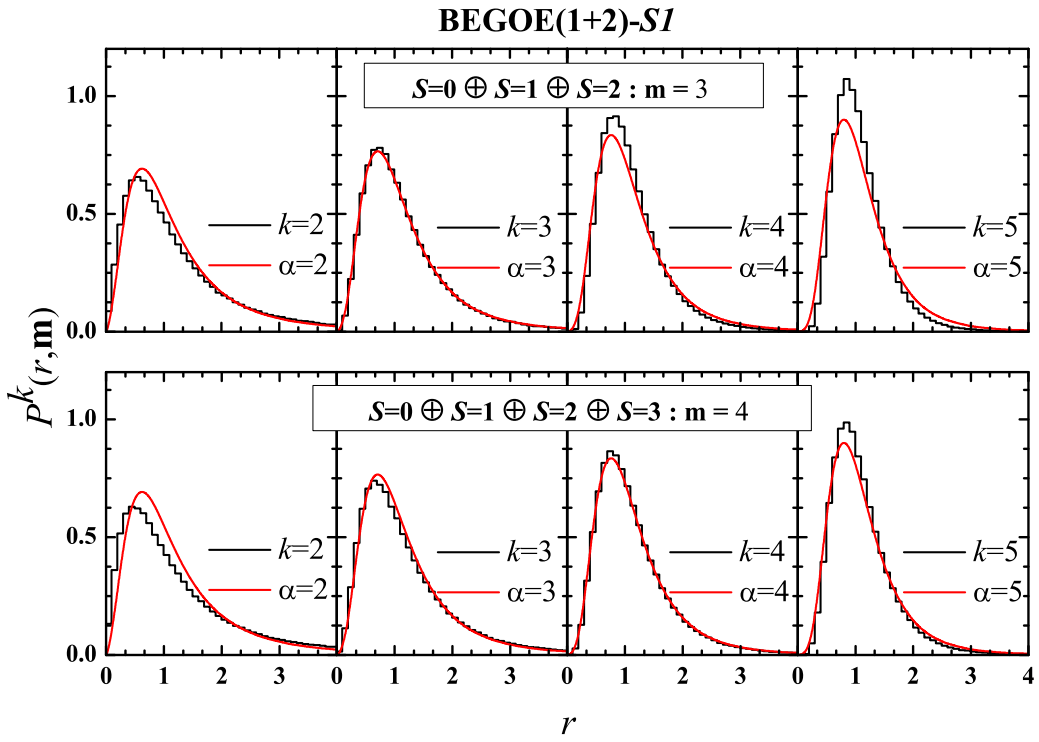

Figure 3.10: Same as Fig. 3.8 but results are for $\mathbf{m}$ superposed spectra of a 500 member BEGOE(1+2)-$S1$ ensemble. Here $\lambda = \lambda_0 = \lambda_1 = \lambda_2 = 0.2$. Results for $\mathbf{m} = 3$ with spins $S = 0 - 2$ are shown in upper panel and results for $\mathbf{m} = 4$ with spins $S = 0 - 3$ are shown in lower panel. See Fig. 3.8 for details.

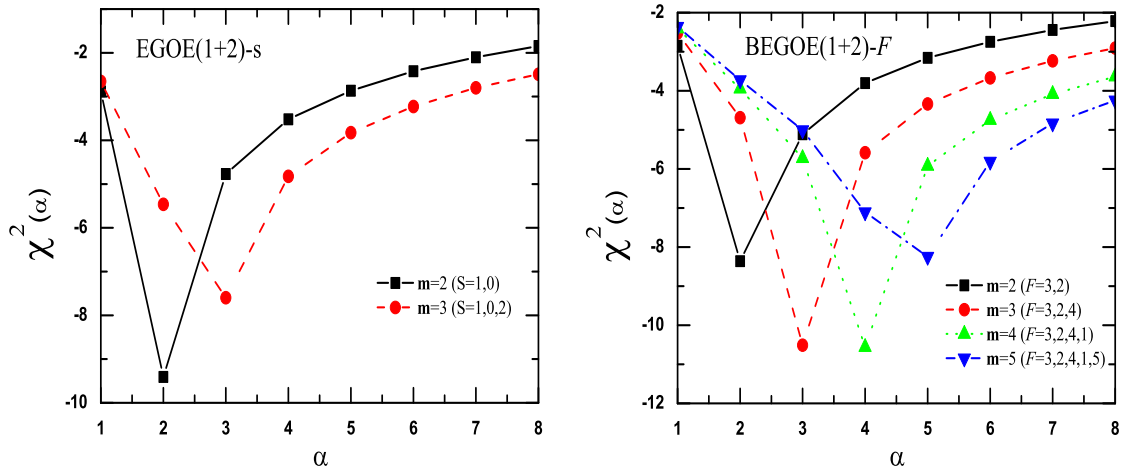

Figure 3.11: Variation in $\chi^2(\alpha)$ vs. α for EGOE(1+2)-$\mathbf{s}$ ensemble (left panel) and BEGOE(1+2)-F ensemble (right panel) for different $\mathbf{m}$ values as mentioned in the panel. In these plots for EGOE(1+2)-$\mathbf{s}$ and BEGOE(1+2)-F, λ is same as in the previous figures. The minimum values of $\chi^2(\alpha)$ indicates $P^k(r, \mathbf{m}) \sim P_\alpha(r)$ for $\mathbf{m}$ superposed spectra.

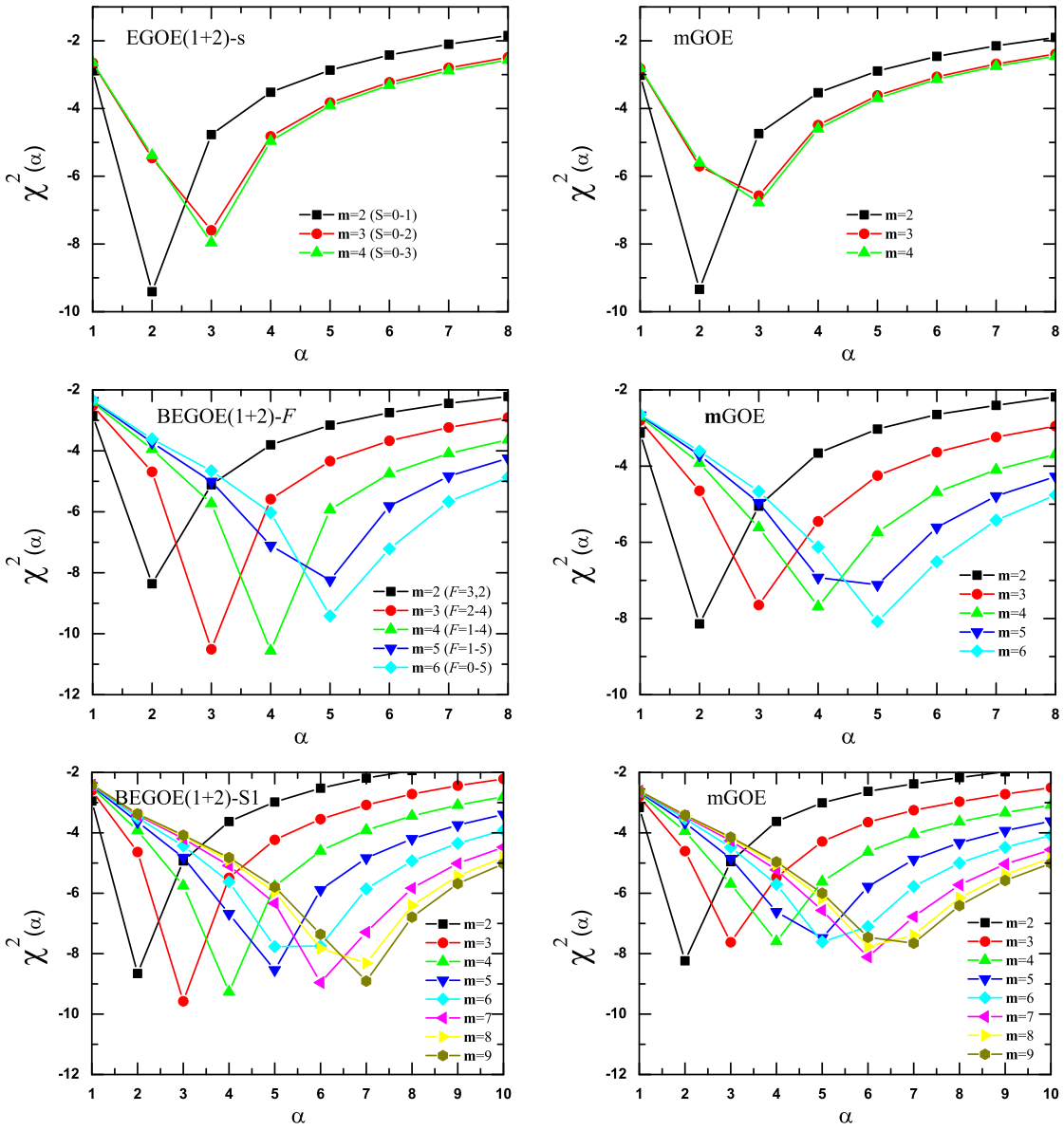

Figure 3.12: Variation in $\chi^2(\alpha)$ vs. α for EGOE(1+2)-$\mathbf{s}$ (top left panel), BEGOE(1+2)-F (middle left panel) and BEGOE(1+2)-$S1$ (bottom left panel) for different $\mathbf{m}$ values as indicated in the panel. Here, λ for EGOE(1+2)-$\mathbf{s}$, BEGOE(1+2)-F and BEGOE(1+2)-$S1$ is same as in previous figures. Right panel represents variation in $\chi^2(\alpha)$ vs. α for superposed $\mathbf{m}$GOE spectra of exactly same dimensions corresponding to results in the left panel for EGOE(1+2)-$\mathbf{s}$, BEGOE(1+2)-F and BEGOE(1+2)-$S1$ respectively. See text for further details.